JOURNAL OF MATERIALS SCIENCE 23 (1988) 2157–2166

The solidification process of highly undercooled bulk Cu–O melts

KOJIRO F. KOBAYASHI, PAUL HIDEO SHINGU
Department of Metal Science and Technology, Kyoto University, Yoshida, Sakyo-ku, Kyoto 606, Japan

The effect of undercooling on grain structure was investigated in pure copper and alloys up to Cu ~ 0.39 wt% O (eutectic composition), in which grain refinement does not occur at any degree of bath undercooled when the oxygen content is less than 300 p.p.m. Grain refinement occurs in these alloys when the oxygen content exceeds about 300 p.p.m. and the undercooling prior to nucleation exceeds 100 K without quenching. Fragmentation affects primary, secondary and tertiary dendrite arms during and after recalescence. Quenching after recalescence at various solidification times retains transient grain structures. When the sample, which should have achieved complete grain refinement by furnace cooling, is quenched immediately after nucleation, the structure shows a trace of radiating fan-shaped grains originating from a single point of nucleation.

1. Introduction

A highly undercooled bulk melt can be obtained by melting the metal under a glass slag. The glass prevents the metal from being nucleated by the crucible walls and probably removes most of the impurities which act as active nucleants in the melt [1–3].

When bulk samples of alloy melts are undercooled, grain refinement of the resultant ingots is observed within limited ranges of undercooling, commonly less than 80 K and greater than 150 K [4–6]. Between these ranges of coarse-grained structure is exhibited. Some representative observations of grain structure are summarized in Fig. 1, which shows the maximum undercooling recorded for bulk melts, which in most cases were of the order of 100 to 200 g.

In iron and nickel-base alloys, an abrupt grain refinement occurs beyond a critical amount of undercooling [9–11]. The transition to the fine grains does not occur in copper containing less than 0.0.15 wt % O and below 0.25 wt % S [14], or when the deoxidizers phosphorus [4, 15] or tin [16] are present, but nickel in iron [9–11] or copper in nickel [11] or silver in copper [17] do not affect the transition.

Major changes in grain structure occur very rapidly during solidification by a coarsening process [18] and the extent of the changes is governed by the total time of solidification, which can be shortened by quenching. The mechanisms of grain refinement are related to solute content and type of solute.

This paper reports a study of the systematic changes in grain structure of hypo-Cu–O alloys as functions of the degree of undercooling and solidification time after nucleation. The alloy chosen, Cu–O, has a long freezing range which would permit dendrite arm coarsening, and the ingots were quenched after recalescence at various solidification times to understand the process of solidified structure formation from highly undercooled melts.

2. Experimental procedure

Materials were oxygen-free high-conductivity copper (99.999%) and Cu_2O. Ingots of about 30 g were melted, alloyed and undercooled under a glass slag in silica crucibles supported in a vertical resistance tube furnace (Fig. 2). The alloying procedure was first to melt pieces of slag glass in the crucible, maintained above the melting point of copper. Weighed pieces of copper were pressed into the molten glass and covered promptly to minimize oxidation. The thermocouple was Pt/Pt–13% Rh. The wires, of 0.1 mm diameter, were insulated from each other by silica protective sheaths and calibrated at the freezing point of the copper. When nucleation was obtained, the specimen was allowed to recalesce naturally into the equilibrium solid plus liquid region. The crucible was lowered into a water bath to quench the sample at various solidification times.

Oxygen contents were determined by coulometric titration using a carrier-gas fusion technique for the solidified specimen. This equipment was manufactured by Strölein (W. Germany).

The crucible and glass were parted from the specimen in hydrofluoric acid. Surfaces and polished sections were etched in acid ferric chloride reagent. Orientations were determined with back-reflection X-ray diffraction patterns with unfiltered copper radiation at 10 kV.

3. Results and discussion

3.1. Relationship between oxygen content, undercooling and macrostructure

The sample compositions, undercooling levels and observed grain structures are listed in Table I. Fig. 3

0022–2461/88 $03.00 + .12

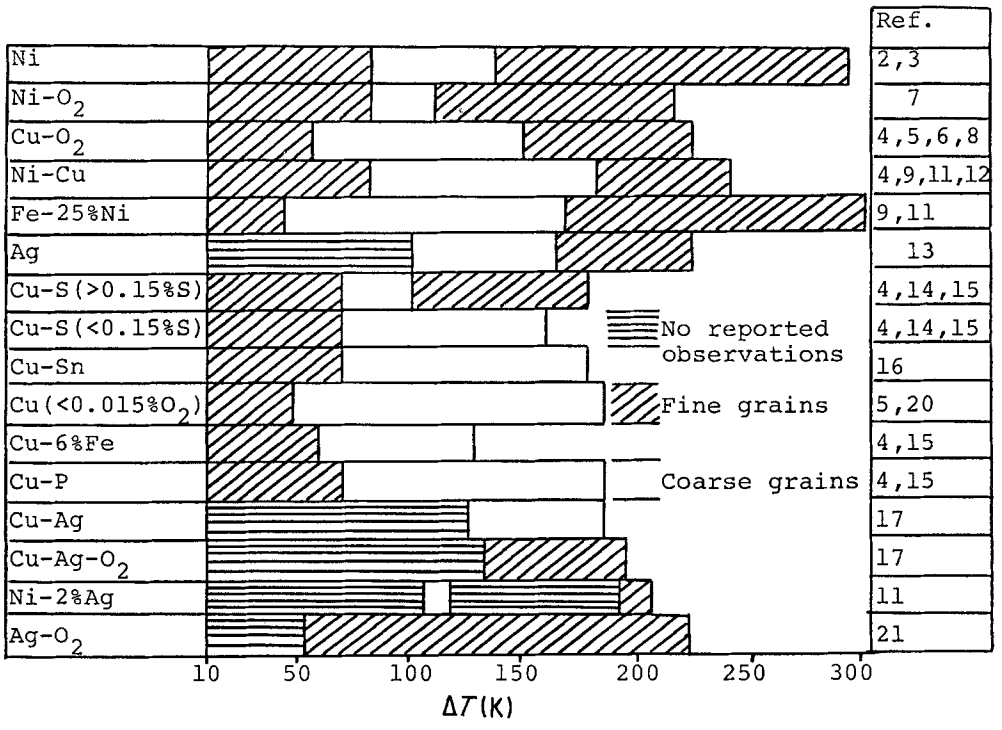

Figure 1 Summary of some representative observations of grain structure in undercooled metals. Maximum recorded undercooling is shown by the length of each bar.

TABLE I Structural features of undercooled Cu–O alloy*

Sample No.	Max. undercooling ΔT (K)	$t_q - t_0$ (sec)	f_{sq} (%)	Oxygen content (p.p.m.)	Grain structure
1	140	3.0	36.0	20	F
2	123	15.0	57.6	18	C
3	120	3.8	32.8	18	C
4	100	8.5	37.5	19	F
5	103	10.0	39.1	25	C
6	88	8.0	33.3	21	C
7	80	2.9	22.4	21	C
8	76	7.3	28.7	23	F
9	78	13.0	39.7	25	C
10	56	3.4	17.2	26	C
11	225	12.0	84.4	29	F
12	45	2.0	12.8	31	C
13	110	33.0	100.0	40	F
14	67	3.2	19.4	37	C
15	15	20.0	33.6	40	C
16	99	2.0	24.8	60	F
17	82	1.8	20.5	78	C
18	22	1.9	7.6	78	C
19	212	3.1	54.1	105	F
20	160	1.0	35.5	164	F
21	120	2.1	29.7	258	F
22	65	8.0	26.7	260	F
23	20	20.0	32.5	260	C
24	140	11.0	56.7	320	F
25	148	1.0	33.5	364	F
26	73	1.4	17.8	1025	F
27	60	9.0	27.0	1260	E
28	32	13.0	25.2	1800	C
29	16	60.0	100.0	1220	C
30	130	2.0	32.0	2400	E
31	125	7.8	43.2	2590	E

*$t_q - t_0$ = solidification time, f_{sq} = fraction solid at the time of quenching, C = coarse grains, F = fan-shaped grains radiating from one nucleation centre, E = fine, equiaxed grains, randomly oriented.

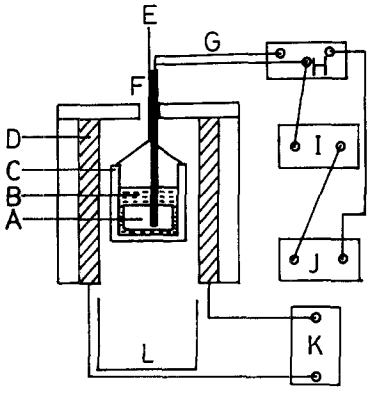

Figure 2 Experimental apparatus for glass slag method: (A) sample, (B) glass slag, (C) crucible, (D) furnace, (E) wire, (F) silica sheath, (G) thermocouple, (H) temperature compensator, (I) reference voltage unit, (J) recorder, (K) power supply, (L) water bath.

shows grain structure types related to oxygen content and undercooling (ΔT).

3.2. Typical macrostructures of undercooled Cu–O ingots

Solidification structure is strongly influenced by the amount of solute content and the degree of undercooling at nucleation. The results obtained can be classified into three different types: C, coarse grains; E, equiaxed grains and F, fan-shaped grains [14]. Three typical grain structures are shown in Fig. 4.

The fan-shaped structure always shows a point of nucleation somewhere in the ingot from which the crystals radiated. X-ray study shows that all the crystals in some ingots are related via twinning events and grow in ⟨1 0 0⟩ directions [14, 16, 19].

In considering nucleation from a melt, most of the effective heterogeneous nucleants are removed from the highly undercooled melt so that nucleation occurs at undercooling (ΔT) below the liquidus of the order of $\Delta T = 0.2T_L$, where T_L is the liquidus temperature. Under these conditions the interfacial interaction between nucleus and heterogeneous nucleant must be very small indeed and, from the evidence described above, it might be expected that the nuclei could take the form of multiply twinned, equiaxed particles with low-energy ⟨1 1 1⟩ surface facets. Experiments on the undercooling of fcc metals regularly produce ingots in which all grains grow from a single nucleation centre and more-or-less complex twin relationships exit between the grains [14, 15, 16, 20], so that it must be assumed that crystallization commenced from a single multiply-twinned nucleus [22–24].

3.3. Estimation of the solid fraction at quenching

The solid fraction (f_{sq}) at various quenching times (t) can be calculated approximately by the use of the schematic cooling curve shown in Fig. 5. f_{sq} is expressed as a function of the degree of undercooling, ΔT ($= T_m - T_n$), and the time from start of nucleation, t, where T_m and T_n are the temperatures of melting point and nucleation, respectively. With the notation of t_e and f_s^* as solidification time for 100% solid and fraction of solid after recalescence to solidus, respectively, f_{sq} is given by the equation

$$f_{sq} = f_s^* + (1 - f_s^*)\frac{t}{t_e} \quad (1)$$

If it is assumed that the liquid is cooled to a uniform temperature, isolated so that no heat may enter or leave it, and then nucleated, the total amount of solid, f_s^*, that can be formed can be calculated from the latent heat of fusion, L, the specific heats, C_l and C_s, and ΔT. When L, C_l and C_s are assumed independent

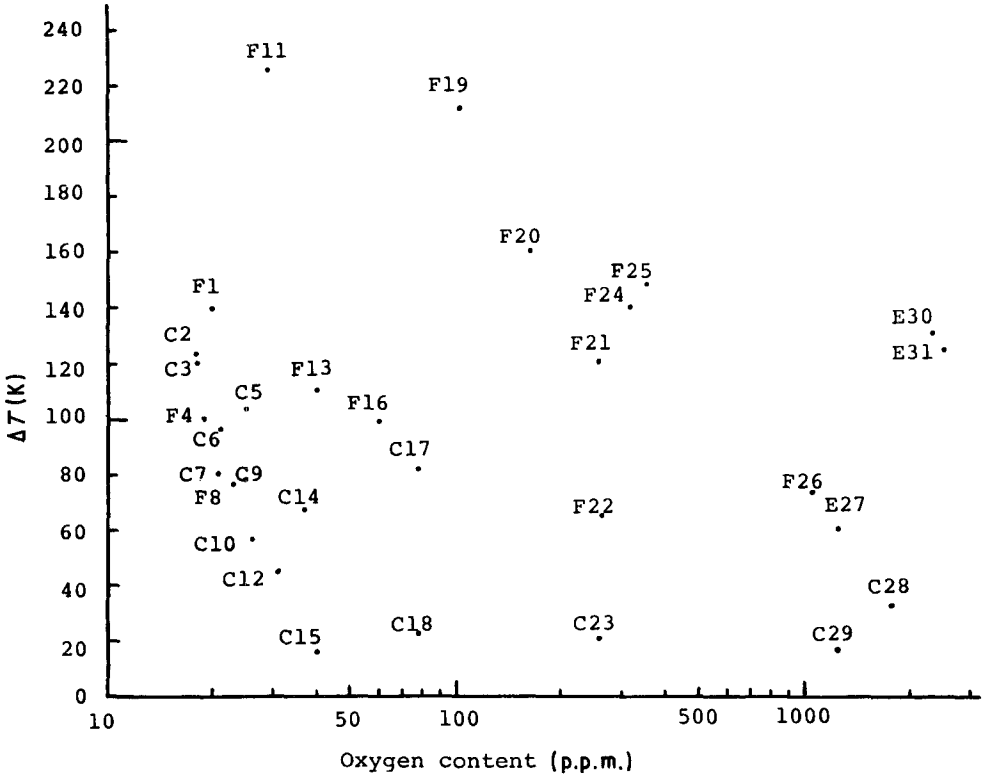

Figure 3 Grain structure types related to oxygen content and degree of undercooling at nucleation: (C) coarse, (F) fan-shaped, (E) equiaxed. Numbers refer to Table I.

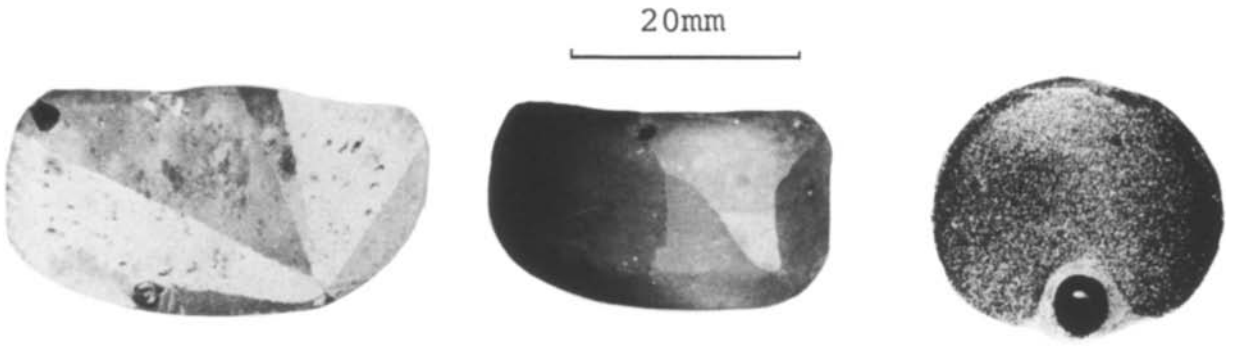

Figure 4 Photographs of three typical types of grain structure. (a) Type F (Sample 11) shows the fan-shaped grains radiating from a single point of nucleation. The grains are related by twinning events. (b) Type C (Sample 12) shows a coarse-grained structure. (c) Type E (Sample 31) shows a fine, equiaxed grain structure.

of temperature, f_s^* is given by the equation

$$f_s^* = \frac{2C_l\Delta T}{2L - (C_l - C_s)\Delta T} \quad (2)$$

The recalescence time is very small compared to the solidification time, and at high undercoolings it is negligible in comparison with total the solidification time. On the other hand, the cooling rate of furnace is constant in this work, namely

$$\frac{dT_f}{dt} = -a \qquad a = 3.25\,\mathrm{K\,sec^{-1}} \quad (3)$$

where T_f is the furnace temperature.

The real heat balance between sample and furnace is

$$\frac{\partial(C\varrho VT)}{\partial t} = VL\varrho\frac{\partial f_s}{\partial t} - Ah(T - T_f)$$

where, V, ϱ, A, h, C and T are volume, density, surface area, heat transfer coefficient, specific heat and temperature of the specimen, respectively. Under the conditions of this work, h was roughly determined as $0.02\,\mathrm{cal\,cm^{-2}\,K^{-1}\,sec^{-1}}$ ($0.08\,\mathrm{J\,cm^{-2}\,K^{-1}\,sec^{-1}}$) from preliminary experiments. In this work, solidification time from the beginning of recalescence to quench was employed as a parameter of the solid fraction at the quenching. By the use of Fig. 5, the above equation can be simplified as following:

$$V(1 - f_s^*)L\varrho = \int_{t_0}^{t_e} Ah(T_m - T_f)\,dt \quad (4)$$

Calculations from Equations 1, 2, 3 and 4 lead to the following expression for f_{sq}:

$$f_{sq} = \frac{2C_l\Delta T}{2L - (C_l - C_s)\Delta T} + at \times \left(\frac{1 - 2C_l\Delta T}{2L - (C_l - C_s)\Delta T}\right)\Big/\left\{-\Delta T + \left[(\Delta T)^2 + \frac{2aV\varrho L}{Ah}\left(1 - \frac{2C_l\Delta T}{2L - (C_l - C_s)\Delta T}\right)\right]^{1/2}\right\}$$

Hence we can get a parameter of solid fraction, f_{sq}, at a given quenching time during solidification as shown in Table I.

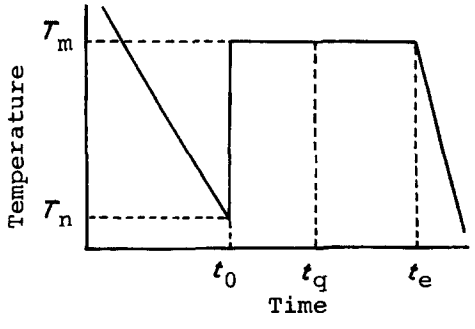

Figure 5 Schematic cooling curve.

3.4. Nucleation and growth in the highly undercooled melts

Classical nucleation theory gives the following expression for the nucleation frequency [25–29]:

$$J(T) \doteqdot \frac{10^{30}}{\eta}\exp\left[-\frac{16\pi\alpha^3\beta}{3}\left(\frac{T_r}{1 - T_r}\right)^2\right] \quad (5)$$

where η = viscosity of liquid, T_r = reduced temperature ($= T/T_m$) and T_m = equilibrium melting point; α is a factor which depends on the atomic arrangement at the interface with a value close to unity, and β is the entropy change due to solidification in units of the gas constant.

The growth rate of the crystal nuclei is given by molecular kinetic considerations assuming that the atomic transport across the interface region, which usually is assumed as several atomic diameters in thickness, takes place by a diffusive process as follows:

$$V(T) = \frac{K}{\eta(1 - T_r)} \quad (6)$$

where $K = a^3L/3\pi\lambda$ and a = atomic diameter, L = heat of fusion, λ = interface thickness.

The temperature dependence of viscosity in the undercooled liquid region is represented assuming a Tamman and Hesse type of relation.

$$\log\eta = A + \frac{B}{T - T_\infty}$$

where A, B and T_∞ are constants which are determined assuming $\eta = 10^{13}$ poise (10^{12} Pa sec) at $T = T_g$ (glass temperature); η is the value for the Arrhenius relation at $T = T_m$ and $d(\log\eta)/d(1/T)$ is the slope of the Arrhenius relation at $T = T_m$.

The calculated results for the nucleation and growth

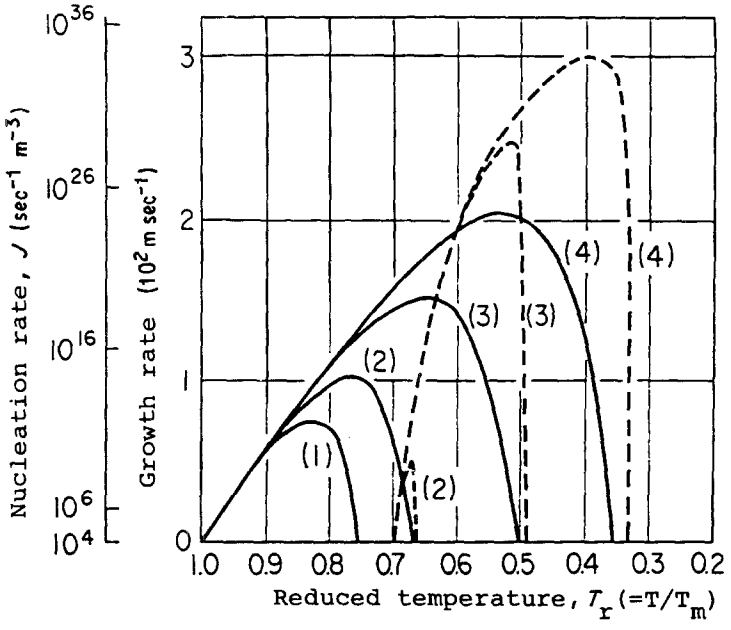

Figure 6 Calculated copper crystal (– – –) nucleation and (——) growth rates as a function of reduced temperature T_r ($= T/T_m$) based on the Equations 5 and 6. Values of $T_{rg} = T_g/T_m$: (1) 3/4, (2) 2/3, (3) 1/2, (4) 1/3.

rate for pure copper as a function of reduced temperature are given in Fig. 6.

The general form of the fraction of phase transformation may be given as

$$-\ln(1 - X) = \frac{4\pi}{3}\int_0^t J(\theta)\left[\int_\theta^t V(\beta)\,d\beta\right]^3 d\theta \quad (7)$$

where $J(\theta)$ is the nucleation frequency, $V(\beta)$ is the linear growth velocity, X the crystallized fraction and t the time after the melting point is passed during cooling.

The temperature–time–transformation (TTT) diagram gives the time necessary to reach a given crystallized fraction by isothermal holding at a given temperature. The glass slag method is a continuous cooling process, hence the critical degree of undercooling may better be estimated by the continuous-cooling-tranformation (CCT) diagram which takes the cumulative effect of nucleation and growth during cooling into account. There are methods to estimate the CCT diagram from a knowledge of the TTT diagram, for example the use of the "additivity" rule which assumes that the cumulative effect of incubation time during cooling is additive [30] or the use of the semi-empirical rule known as the Grange–Kiefer method [31].

Examples of calculated TTT and CCT diagrams for the case of pure copper are given in Fig. 7. From Fig. 7 the maximum undercooling for homogeneous nucleation should be 330 K at the cooling rate of 3.2 K sec^{-1} employed in this work. These calculations are based on many assumptions involved in the nucleation and growth theories. Moreover, data for the viscosity of undercooled liquid are not known for metals, hence at the present stage not too much quantitative accuracy should be expected for the calculated critical undercooling corresponding to a given cooling rate.

However, the relationships among solid fraction, undercooling and cooling rate can be roughly estimated by this calculation.

3.4. Formation of solidified structure from highly undercooled melts

3.4.1. Oxygen content < 300 p.p.m.

When the oxygen content is less than 300 p.p.m., grain refinement does not occur at any degree of undercooling. For $\Delta T < 70$ K, solidification occurs from plural nucleation points and makes a coarse-grained structure.

Fan-shaped grains radiating from a single nucleation centre, in which complex twin relationships

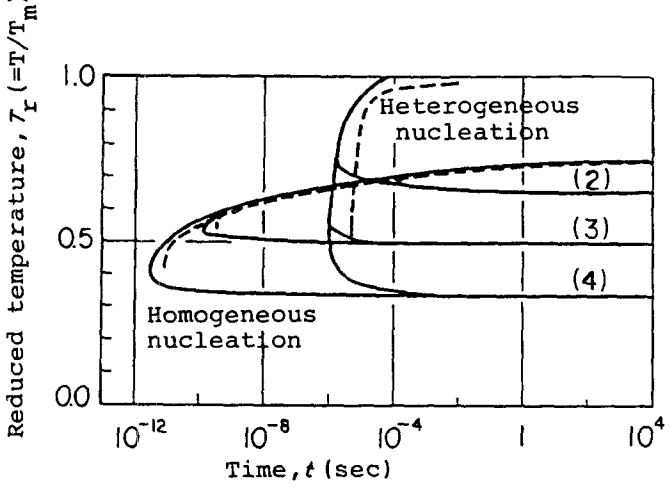

Figure 7 Calculated (——) TTT and (– – –) CCT diagrams for the crystallized fraction of 10^{-6} for copper. Comparison of CCT diagrams for the homogeneous and heterogeneous nucleation cases. 10^5 m^{-3} heterogeneously nucleated crystals are assumed at $T_r = 1$ for the heterogeneous nucleation case. Values of T_{rg}: (2) 2/3, (3) 1/2, (4) 1/3.

exist, start to appear at about $\Delta T = 70\,K$, and for $\Delta T > 100\,K$, in almost all specimens, solid nucleates at a single point in the melt. Needle-like dendrite spines grow from the nucleation centre at high velocity, radiating in $\langle 1\,0\,0 \rangle$ directions [14].

Grain refinement is not observed at large undercoolings, though Walker [3] reported that abrupt grain refinement may occur beyond a critical amount of undercooling, about 175 K. This fact cannot be explained by Walker's cavitation pressure-wave mechanism since the effects of such a mechanism would be independent of the alloy composition and be greatest at the largest undercooling.

3.4.2. Oxygen content > 300 p.p.m.

When the mass percentage of oxygen is more than 300 p.p.m., mainly four factors, such as

(a) solute distribution coefficient, k,
(b) solute content,
(c) solidification time and
(d) growth rate

may be related to the processes of structure formation.

3.4.2.1. Solute distribution coefficients, k. The k values are 0.006 for sulphur, 0.013 for oxygen, 0.2 for tin and 1.4 for iron [32]. Small k-value elements added to the melt make the growing crystal surface less stable. The perturbation may cause the formation of side-branches on the spine at the earlier stages of growth. It enhances the frequency of secondary dendrite arm formation per unit length and makes finer secondary arms. In the case of the dendritic growth from the undercooled melt, the solute is rejected not forward but sideways or backward, because the growth rate is large and the tip radius of the primary is small. The effect of small k value on these processes could be twofold in that the necks at secondary dendrite arm junctions become finer and easier to detach, and the solute-rich liquid around the dendrite would create a higher solid–liquid interfacial energy.

There is some clear evidence that the k value influences the formation of solidified structure from highly undercooled melts ($\Delta T > 70\,K$). When tin, which has a larger k value (0.2) for copper, was alloyed to copper, it showed no fragmentation for $\Delta T > 70\,K$ by changes of the solidified condition such as solidification time, solute content and growth rate, (Mcleod and Hogan [16]).

On the other hand, when sulphur or oxygen which has a one-and-a-half order smaller k value for copper than for tin was alloyed to copper, grain refinement appeared clearly in the range $\Delta T > 60\,K$ in the present work.

3.4.2.2. Solute content. The secondary arm spacing decreases slightly with increasing solute content [33]. As the rejected solute content increases around the dendrite by the progress of the solidification, the necks become finer with large radii at the junctions. This tendency is enhanced in solute-rich specimens compared with in poor ones.

Fig. 8 shows the effect of oxygen content on the macrostructure initiated from a single nucleation centre. Both the degree of undercooling (at nucleation) and the solid fraction (at quenching) were kept nearly same for each sample. Though a trace of a single point of nucleation is revealed by quenching during solidification for each sample, the higher oxygen content samples should achieve complete grain refinement after full solidification.

The dependency of grain size, d, on oxygen content for samples with nearly the same degree of undercooling and solid fraction is plotted in Fig. 9, in which data are employed from Fig. 8. Grain size, d, is measured at a position about 4 mm from the point when the nucleation centre can be observed. The grain size is estimated by the number of intercepts per unit length on a section perpendicular to growth direction. For equiaxed grains a wide variety of test-line patterns is employed, so as to obtain a measurement free of anisotropy effects.

3.4.2.3. Total time of solidification. Kattamis and Flemings [9, 11] showed, using an Fe–25% Ni alloy, that major changes in grain structure occur very rapidly during solidification by a coarsening process and that the extent of the changes is governed by the total time of solidification, which can be shortened by quenching.

Fig. 10 shows the changes of structure with solid

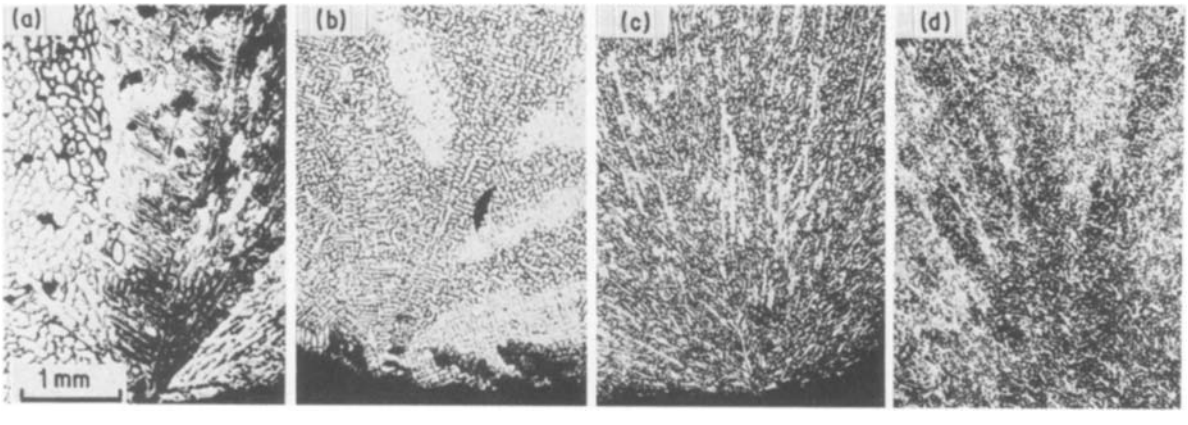

Figure 8 The effect of oxygen content on the macrostructure of a single nucleation centre. Both the degree of undercooling (at the time of nucleation) and the solid fraction (at the time of quenching) were kept nearly the same for each sample. (a) Sample No. 1, (b) Sample No. 20, (c) Sample No. 25, (d) Sample No. 30. For properties see Table I.

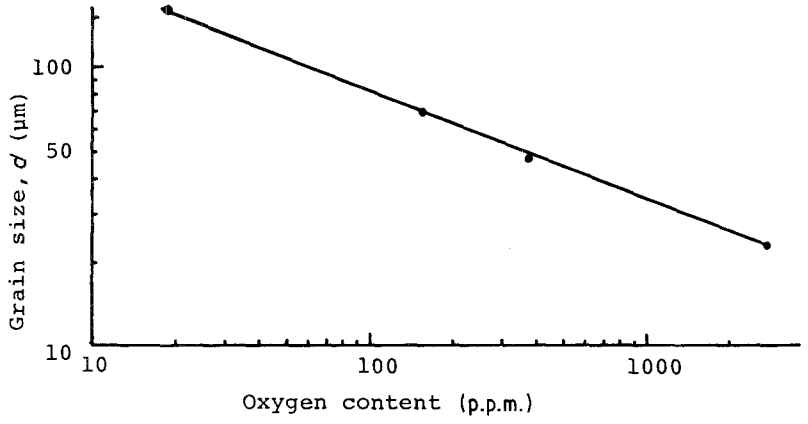

Figure 9 Dependence of grain size, d, on the oxygen content for samples with nearly the same degree of undercooling (at nucleation) and solid fraction (at quenching).

fraction at quenching, for two different oxygen content levels. The samples are nucleated at nearly the same degree of undercooling. The solid fraction at quenching affects the structural change, which is drastic in high oxygen content samples. This fact shows that the solute content is one of important factors, as described in Section 3.4.2.2.

A greater solidification time permits the formation of equiaxed grains, and Samples 25 and 31 contain annealing twins in the structure. New grains are controlled to about the same diameters as the preexisting subgrains by an interdendritic distribution of Cu_2O particles as shown in Fig. 11.

3.4.2.4. Growth rate. The growth rate is found experimentally to be approximately proportional to the square of the degree of undercooling. Fig. 12 shows the effect of the degree of undercooling (at nucleation) on the macrostructure. All the samples were quenched into water at nearly the same solid fraction for two different oxygen content levels. Higher velocity growth from largely undercooled melt makes a finer structure during solidification.

Relationships between the grain size, d, and undercooling (at nucleation), ΔT, are shown in Fig. 13. Data are employed from Fig. 11 and Sample 21. For the lower oxygen level, d is roughly proportional to $(\Delta T)^{-1/2}$ and $d \propto (\Delta T)^{-1}$ for the higher oxygen level.

The micrograph of Sample 22 (Fig. 14) shows a pattern of major grains and subgrain boundaries, with a subgrain size comparable to the grain size of Fig. 11.

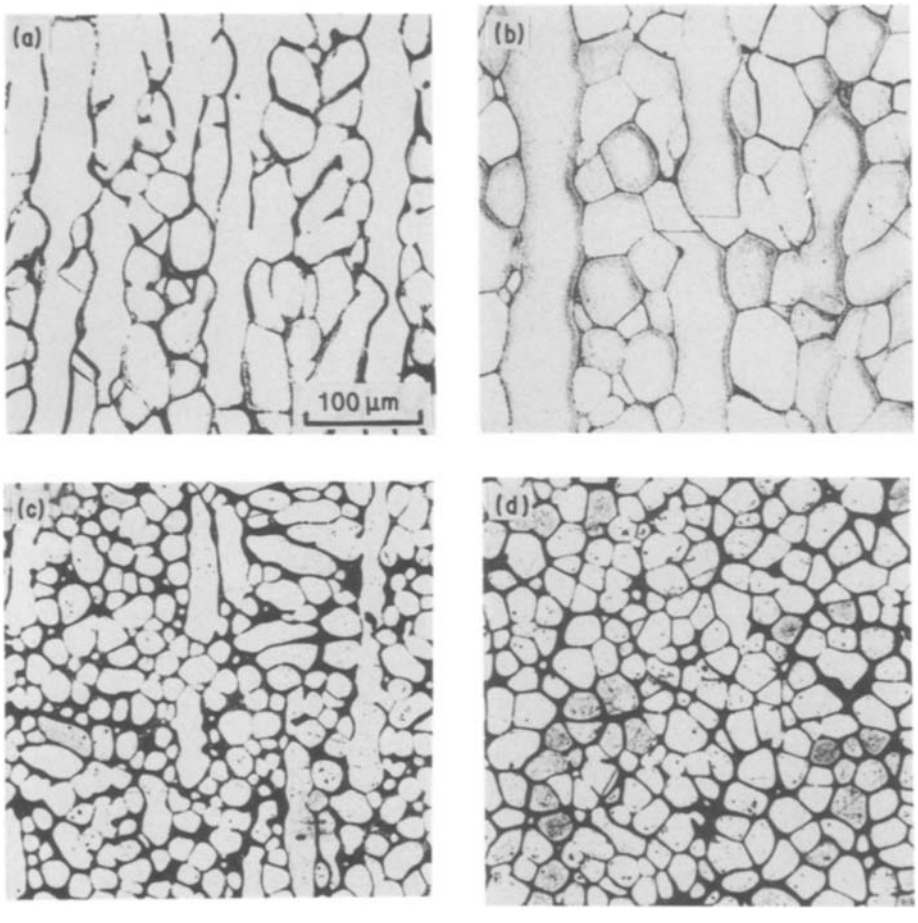

Figure 10 The effect of solid fraction (at the time of quenching) on the microstructure of samples nucleated at nearly the same degree of undercooling is shown for two different oxygen content levels. Lower oxygen content: (a) Sample No. 24, (b) Sample No. 25. Higher oxygen content: (c) Sample No. 30, (d) Sample No. 31. For properties see Table I.

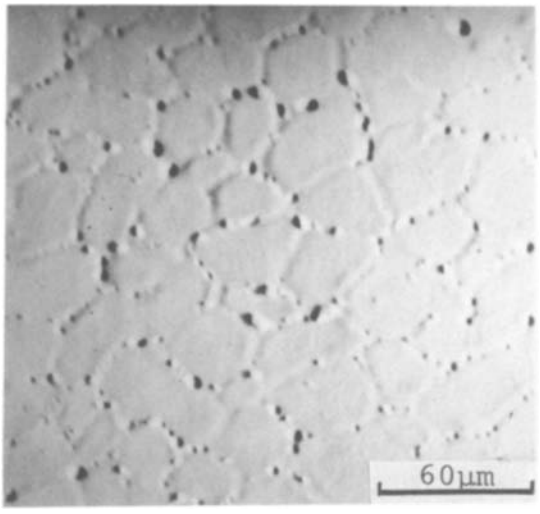

Figure 11 Inderdendritic distribution of Cu_2O particles. The equiaxed grains are subgrains whose boundaries are pinned by oxide particles.

3.5. Grain refinement mechanism

There are three types of explanation for the grain refinement.

Nucleation hypotheses, which propose that each grain nucleates individually from the melt, are based on cavitation theories [3]. These independent nucleation hypotheses have not been disproved, but may be losing credence, although the pressure-wave exists and could certainly be expected to assist in any dendrite fragmentation process.

"Two-stage" hypotheses propose that the equiaxed structure is formed during recalescence by some sort of rearrangement of an array of large dendrites. Kattamis and Flemings [11] showed that a dendrite coarsening process is enough to explain their observations, in which each spheroidal grain is enclosed within a high-solute boundary for Ni–Fe alloys.

It is true that a polygonal grain grows by a recrystallization mechanism from the solid dendrites, with a driving force provided in some way by an excess of oxygen in solution. Substantial grain boundary movement, associated with twin propagation, occurs in the completely solid state and determines the grain boundary pattern finally observed at room temperature [5, 14].

For Cu–O alloys, the following explanation for the appearance of fine-grains may be proposed from the results of the present work.

3.6. Structural changes during solidification

Once nucleation occurs in the highly undercooled melt, needle-like dendrite spines grow from a nucleation centre at high velocity, radiating in ⟨100⟩ directions. The size and morphology of spines are strongly influenced by the solute content and type of solute (k) and the growth rage as shown in Figs 8 and 9. The fragmentation of the first-formed dendrite spines is likely to occur at an early stage of recalescence when the spines are thin and fragile. A possible explanation lies in the rate of rejection of solute away from the dendrite tips as they advance at high

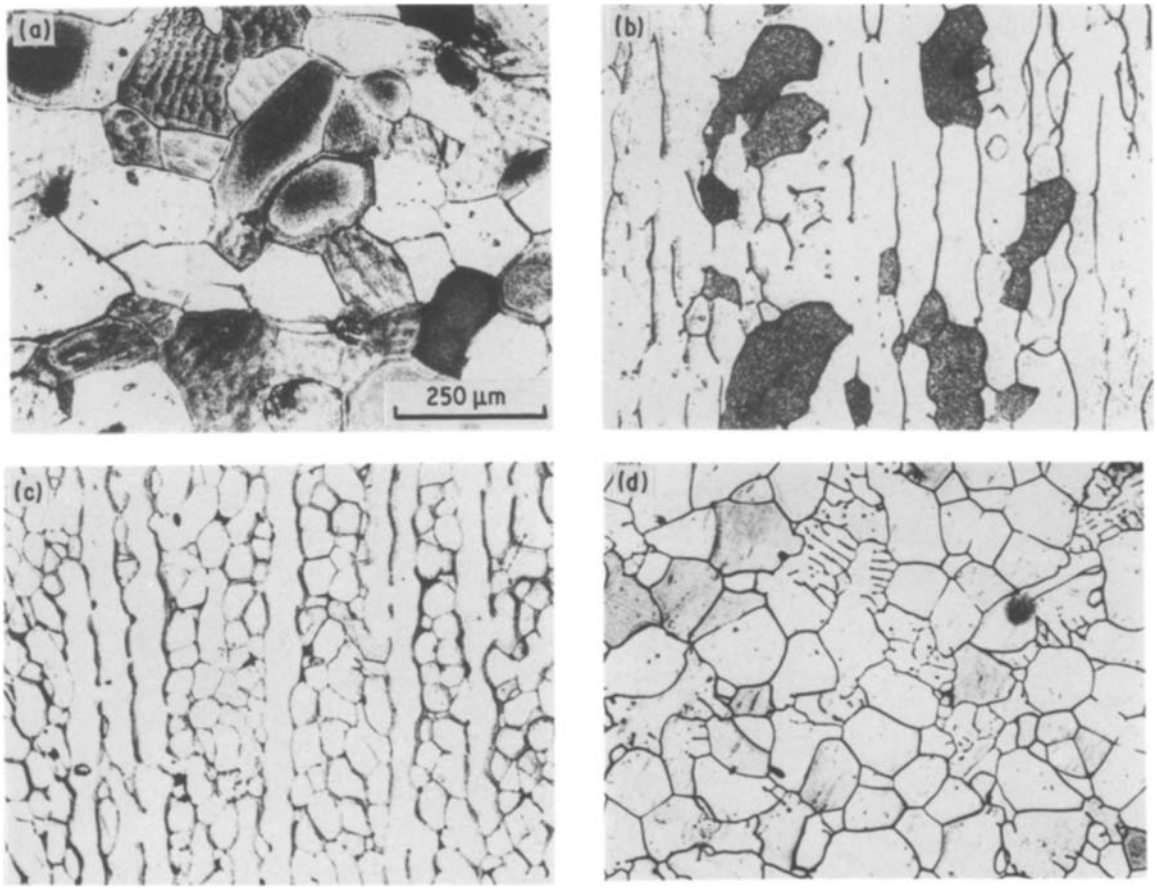

Figure 12 The effect of degree of undercooling on the microstructure of samples (quenched at nearly the same solid fraction) is shown for two different oxygen content levels. Lower oxygen content: (a) Sample No. 23, (b) Sample No. 22, (c) Sample No 25. Higher oxygen content: (d) Sample No. 28, (e) Sample No. 27, (f) Sample No. 30. For properties see Table I.

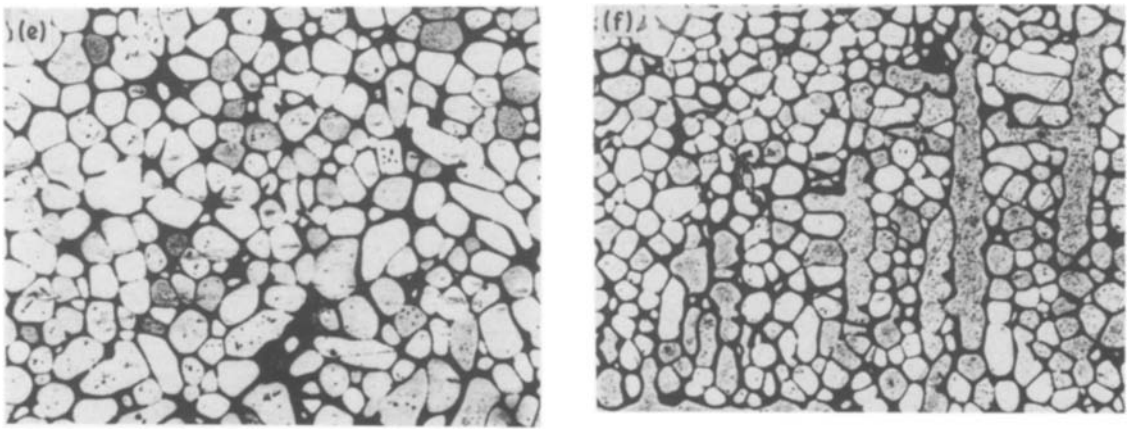

Figure 12 Continued.

velocity. If the growth velocity is too great to permit complete diffusion of solute out of the melt in contact with the advancing tip, some solute trapping may occur in the solid [34], which has nearly zero equilibrium solubility for oxygen. As a result of high-velocity growth after large undercooling, a high energy content of the first-formed structure also can be expected to be built in, in the form of a high population of crystalline defects. These spines would be subject to fracture as a result of any disturbance, such as a pressure wave that results from solidification shrinkage.

At earlier stages, the spine forms secondary and tertiary arms with an inter-arm spacing which coarsens progressively with time. A substantial number of side-arms must certainly be detached by coarsening and remelting processes [35] and the smallest of these will be free to move and rotate in the melt. The shape of the arms, which is determined by solute content, type of solute and growth rate, is a most important factor for structural change during solidification. These facts appear in Figs 8, 10 and 12. With increasing solidification time, the structure changes gradually as shown in Fig. 10.

There is another fragmentation mechanism, called "self-buckling". As a dendrite grows freely into a melt, solidification shrinkage gives rise to a flow of liquid past the growing tips in a direction opposite to the growth direction. This flow has been predicted to become considerable when undercooling exceeds 15 K [36] and could be sufficient to fracture growing side-arms and rotate them to give randomly oriented fine grains.

The subgrain structure (Fig. 14) so formed is replaced by randomly oriented equiaxed grains by a recrystallization process completed within a few seconds after nucleation. The replacement of the initial structure resembles solid-state recrystallization but occurs in the presence of liquid phase. Rapid recrystallization of a coarse dendritic structure containing subgrains and interdendritic precipitates of Cu_2O has happened. It is possible that the driving force for recrystallization in this case is augmented by a high level of supersaturation due to oxygen and that discontinuous recrystallization occurs. In the last stages of solidification, precipitation of Cu_2O pins the grain boundaries and ensures that the final grain size will be comparable with the dendrite element size (Fig. 11).

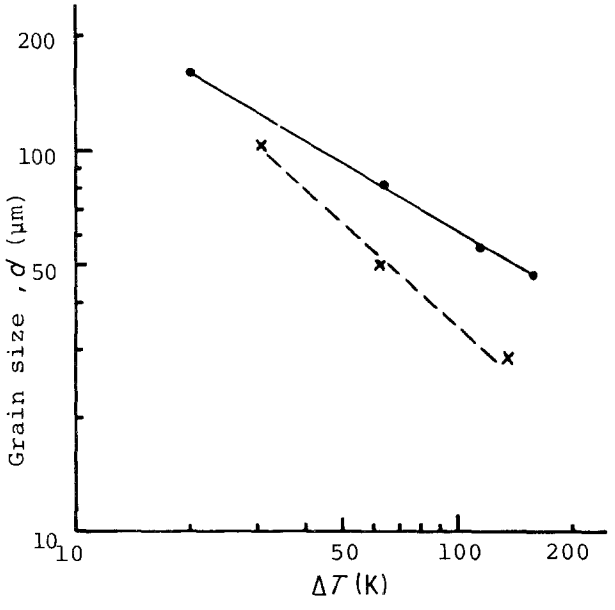

Figure 13 Relationships between size and undercooling ΔT (at the time of nucleation) for (×) high and (●) low oxygen content levels. The solid fraction (at quenching) for each sample is nearly the same.

4. Conclusions

1. The effect of undercooling (ΔT) on grain structure was investigated in pure copper and alloys up to Cu ~ 0.3 wt % O (eutectic composition), in which grain refinement does not occur at any degree of

Figure 14 Micrograph of Sample 22 showing etch pits which belong to two differently orientated grains. Each grain has subgrain boundaries.

undercooling when the oxygen content is less than 300 p.p.m.

2. Grain refinement occurs in undercooled Cu–O alloys when the oxygen content exceeds about 300 p.p.m., and undercooling prior to nucleation exceeds 100 K without quenching after recalescence.

3. Quenching after recalescence at various solidification times retains transient grain structures. Some of the features are as follows:

(a) Crystallization initiates from a single point of nucleation, even when a randomly oriented equiaxed grain structure is formed after full solidification.

(b) At the initial stage, a crystal grows from a nucleus with needle-shaped dendrite spines at high velocity in $\langle 1\,0\,0 \rangle$ directions to the ingot boundaries.

(c) At the next stage, secondary and tertiary dendrite arms which grow after the recalescence become misoriented by coarsening and remelting processes to form subgrains.

(d) When the oxygen content exceeds a critical value, the subgrains are replaced by randomly oriented grains in a recrystallization process.

(e) The new grains are controlled to about the same diameters as the pre-existing subgrains by an interdendritic distribution of Cu_2O particles.

References

1. G. L. F. POWELL and L. M. HOGAN, *J. Inst. Metals* **93** (1964–65) 505.
2. J. FEHLING and E. SCHEIL, *Z. Metallkde* **53** (1962) 593.
3. J. L. WALKER, in "Physical Chemistry of Process Metallurgy", Part II (Interscience, New York, 1961) p. 845.
4. R. T. SOUTHIN and G. M. WESTON, *J. Aust. Inst. Metals* **19** (1974) 93.
5. G. L. F. POWELL and L. M. HOGAN, *Trans. Met. Soc. AIME* **242** (1968) 2133.
6. A. J. McLEOD, *J. Aust. Inst. Metals* **16** (1971) 124.
7. B. L. JONES and G. M. WESTON, *ibid.* **15** (1970) 189.
8. *Idem, ibid.* **15** (1970) 167.
9. T. Z. KATTAMIS and M. C. FLEMINGS, *Mod. Casting* **52** (1967) 97.
10. T. Z. KATTAMIS, *J. Cryst. Growth* **34** (1976) 215.
11. T. Z. KATTAMIS and M. C. FLEMINGS, *Trans. Met. Soc. AIME* **236** (1966) 1523.
12. L. A. TARSHIS, J. L. WALKER and J. W. RUTTER, *Met. Trans.* **2** (1971) 2589.
13. G. L. F. POWELL, *J. Aust. Inst. Metals* **10** (1965) 223.
14. K. KOBAYASHI and L. M. HOGAN, *Metals Forum* **1** (1978) 165.
15. R. T. SOWTHIN and G. M. WESTON, *J. Aust. Inst. Metals* **18** (1973) 74.
16. A. J. MCLEOD and L. M. HOGAN, *Met. Trans.* **9A** (1978) 987.
17. G. L. F. POWELL and L. M. HOGAN, Report on Project No. 93 (International Copper Research Association, New York, 1967) p. 17.
18. T. Z. KATTAMIS and S. SKOLIANOS, in "Rapidly Quenched Metals" Vol. 1, edited by S. Steeb and H. Warlimont, (Elsevier, B.V., 1985) p. 51.
19. A. J. McLEOD and L. M. HOGAN, *J. Cryst. Growth* **8** (1971) 61.
20. B. L. JONES and G. M. WESTON, *J. Mater. Sci.* **5** (1970) 843.
21. G. L. F. POWELL and L. M. HOGAN, *Trans. Met. Soc. AIME* **245** (1969) 407.
22. S. INO, *J. Phys. Soc. Jpn* **21** (1966) 346.
23. S. INO and S. OGAWA, *ibid.* **22** (1967) 1365.
24. K. KOBAYASHI and L. M. HOGAN, *Phil. Mag. A* **40** (1979) 399.
25. D. TURNBULL, *J. Appl. Phys.* **21** (1950) 1022.
26. G. M. POUND and V. K. LAMER, *J. Amer. Chem. Soc.* **74** (1952) 2323.
27. Y. MIYAZAWA and G. M. POUND, *J. Cryst. Growth* **23** (1974) 45.
28. F. SPAEPEN, *Acta Metall.* **23** (1975) 729.
29. F. SPAEPEN and D. TURNBULL, in Proceedings of 2nd International Conference on Rapidly Quenched Metals, Section 1, edited by N. J. Grant and B. C. Giessen (MIT Press, Cambridge, 1976) p. 205.
30. J. W. CAHN, *Acta Metall.* **4** (1956) 572.
31. R. A. GRANGE and J. M. KIEFER, *Trans. ASM* **29** (1941) 85.
32. M. HANSEN and K. ANDERKO, "Constitution of Binary Alloys" (McGraw-Hill, New York, 1958).
33. T. OKAMOTO and K. KISHITAKE, *J. Cryst. Growth* **29** (1975) 137.
34. J. C. BAKER and J. W. CAHN, "Solidification", (American Society for Metals, Metals Park, Ohio, 1971) p. 23.
35. K. A. JACKSON, J. D. HUNT, D. R. UHLMANN and T. P. SEWARD, *Trans. Met. Soc. AIME* **234** (1966) 149.
36. W. A. TILLER and S. O'HARA, "The Solidification of Metals", No. 101 (ISI Publications, London, 1967) p. 27.

Received 22 June
and accepted 22 September 1987